Journal of Magnetism and Magnetic Materials 329 (2013) 53–58

Contents lists available at SciVerse ScienceDirect

Journal of Magnetism and Magnetic Materials

journal homepage: www.elsevier.com/locate/jmmm

Cation distribution and magnetic characterization of the multiferroic cobalt manganese Co_2MnO_4 spinel doped with bismuth

Maria Elenice dos Santos [a,b,*], Rafael Aparecido Ferreira [a,b], Paulo Noronha Lisboa-Filho [c], Octavio Peña [b]

[a] Grupo de Materiais Avançados, UNESP—Universidade Estadual Paulista, 17033-360 Bauru, SP, Brazil
[b] Institut des Sciences Chimiques de Rennes, UMR 6226, Université de Rennes 1, A. Du Géneral Leclerc, 35042 Rennes, France
[c] Departamento de Física, Faculdade de Ciências, Universidade Estadual Paulista, 17033-360 Bauru, SP, Brazil

ARTICLE INFO

Article history:
Received 19 June 2012
Received in revised form
26 September 2012
Available online 12 October 2012

Keywords:
Multiferroic materials
Magnetic properties
Ferrimagnetism
Valence fluctuations

ABSTRACT

The structural and magnetic properties of the cubic spinel oxide Co_2MnO_4 (*Fd3m* space group) doped with different concentrations of bismuth, were investigated by X-ray diffraction and SQUID magnetometry. The Bi^{3+} ions entering into the Co^{III} octahedral sites do not alter the effective moment, $\mu_{eff} \sim 8.2\ \mu_B$, whereas both the magnetization $M_{50\ kOe}$ at the highest field (50 kOe) and the field-cooled M_{FC} magnetizations increased when increasing the Bi content. The ferrimagnetic character of the parent compound, Co_2MnO_4, is maintained for all materials although the antiferromagnetic interactions Co^{2+}–Co^{2+} are affected, resulting in higher values of the Curie–Weiss temperature. Due to the large ionic radius of Bi, octahedra distortions occur as well as valence fluctuations of the Mn ions, giving rise to Jahn-Teller effects and enhancing the exchange interactions. The off-center Bi^{3+} ion is responsible of non-centrosymmetric charge ordering and should lead to multiferroïsme conditions for the $Bi_xCo_{2-x}MnO_4$ material.

1. Introduction

Multiferroics materials, in which an electric dipole-moment alignment can be switched by an electric field and conversely the alignment of electron spins can be reversed by a magnetic field, have been the object of a great interest in this last decade because they represent an enormous challenge in materials science [1]. One of the most attractive features on multiferroic materials is the magnetoelectric coupling for which both order parameters (magnetic and electric) are directly coupled [2]. Among these materials, the magnetic oxides crystallizing in the perovskite ABO_3 and spinel AB_2O_4 structures (A and B, cationic positions) are especially interesting because their structural, magnetic and electronic properties can be easily modified by slightly doping their crystal structures [3,4].

Basic ingredients for multiferroïsme are the presence of non-magnetic cations with empty d shells (d^0) located off-center at the oxygen polyhedra (A-sites in perovskites and B-sites in spinels) and the presence of unpaired localized electrons at the B-site: the first ones provide the electric dipole moments for ferroelectricity while the second ones provide the magnetic properties and eventually the ferromagnetic (or antiferromagnetic) interactions. These effects can be obtained by changing the chemical composition and the cation distribution in the perovskite and spinel structures [5]. Many examples of oxide materials crystallizing in the ABO_3 and AB_2O_4 structures can be obtained thanks to the enormous possibilities of substitutions at the A and B positions. Among these materials, cobalt and manganese oxides and in particular, the cobalt–manganese spinel Co_2MnO_4, have been the subject of various structural, electrochemical, optical and magnetic studies, mainly because most of them are potential candidates for multiferroïsme [6–8].

The Co_2MnO_4 spinel oxide crystallizes in a *Fd3m* ($Z=8$) space group, with each cubic unit cell containing Wyckoff positions at 8a tetrahedrically coordinated with the oxygen and 16d octahedrically coordinated with the oxygen, this last one located at 32e positions. This cationic arrangement $(Co)_{8a}[CoMn]_{16d}(O_4)_{32e}$ shows a fully inverted spinel structure with a random distribution of the Co and Mn ions on the tetrahedral and octahedral sites [9,10]. At this point, we should remark that, from here on, we shall adopt the notation Co_2MnO_4 (instead of the more usual for spinels, $MnCo_2O_4$) since, for an inverted spinel structure, the cationic arrangement corresponds to $(Co)[CoMn]O_4$.

Rajeevan et al. synthesized the Bi-doped Co_2MnO_4 multiferroic spinel ($Bi_xCo_{2-x}MnO_4$) by a conventional solid-state reaction and studied their structural, electric and magnetic properties [11]. They showed that Bi insertion just causes a lattice expansion due to the substitution of Co by Bi cations, without any change of the cubic spinel structure [12]. The dielectric constant was enhanced

* Corresponding author at: Institut des Sciences Chimiques de Rennes, UMR 6226, Université de Rennes 1, A. Du Géneral Leclerc, 35042 Rennes, France. Tel.: +33 2 23 23 67 57; fax: +33 2 23 23 67 99.
E-mail address: elenice.dos-santos@univ-rennes1.fr (M.E. dos Santos).

0304-8853/$ - see front matter © 2012 Elsevier B.V. All rights reserved.
http://dx.doi.org/10.1016/j.jmmm.2012.09.070

with the Bi doping, while the ferrimagnetic nature was preserved [12,13]. The nonmagnetic Bi^{3+} ions inserted in the (Co)[CoMn]O_4 structure, with lone pair electrons ($6s^2$), are expected to occupy the Co^{3+} octahedral positions. According to the literature, the Bi^{3+} ion shifts away from the center, distorting the octahedral site and introducing the non-centrosymmetric charge ordering due to covalent bonding with oxygen [14]. The Bi^{3+} ions thus play an important role on the valence fluctuations in the Co_2MnO_4 system since Co and Mn atoms can move between the tetrahedral and octahedral sites, promoting the presence of several oxidation states, $Co^{2+}/Co^{3+}/Co^{III}$ and $Mn^{2+}/Mn^{3+}/Mn^{4+}$, simultaneously coexisting in the material [15]. The structural formula can then be rewritten as (Co)[$Bi_xCo_{2-y-x}Mn_y$]O_4, where cobalt can adopt, depending on its environment, its low-spin (LS Co^{III}, non-magnetic) and/or high-spin configurations. The cation distribution in this system is difficult to determine due to the multiplicity of each cation, with various possible oxidation states and the presence of A–A, A–B, B–B, A–O, B–O bonds, with metal ions showing low and high spin states in an A/B lattice competition [16]. In addition, strong correlations occur between the magnetic sublattices due to the double exchange interactions [17,18] and Jahn-Teller effects [19], this latter distorting the oxygen octahedra surrounding the Mn cations. In order to associate these modifications with the physical properties, a careful study of the various possible interactions between Bi, Co, Mn and O ions should be done. Thus, the design of $Bi_xCo_{2-x}MnO_4$ compounds with well-defined stoichiometries is essential to get better knowledge of the possible mechanisms of magnetoelectric coupling in multiferroic materials.

We report herein on $Bi_xCo_{2-x}MnO_4$ ($x=0.0$; 0.1; 0.2 and 0.3) spinels, synthesized by a chemical route using a polymeric precursors method, where the metallic ions are dispersed in a polymeric gel formed from a mixture of citric acid and a poly-hydroxy alcohol [20]. The large difference of ionic radii between Bi^{3+}(1.17 Å), Co^{3+}(0.65 Å) and Mn^{3+}(0.78 Å) ions may limit the solubility of bismuth in the structure, changing the nominal composition and resulting into the presence of small amounts of spurious oxides [12]. In order to avoid the formation of such transition-metal oxides (like the very stable Bi_2O_3 or BiO), appropriate precursors reagents have been used, as well as a strict pH control during the synthesis.

2. Experimental section

The spinel oxides were synthesized by a modified polymeric precursors method [21] using the corresponding reagents: $MnCO_3$ (Aldrich $>99.9\%$ purity), Bi_2O_3 (Aldrich $>99.9\%$ purity), CoO or $Co(NO_3)_2\cdot 6H_2O$ (both from Aldrich $>99.9\%$ purity), weighed in stoichiometric amounts, to obtain 2 g of material. Firstly, $MnCO_3$, Bi_2O_3, CoO (or Co $(NO_3)_2\cdot 6H_2O$) were dissolved in water at 70 °C by adding HNO_3 (15.2 mol/L, Aldrich $>99.9\%$ purity). A hydrocarboxylic acid ($C_6H_8O_7$, Aldrich $>99.9\%$) was added as a chelating agent in 3:1 proportions (chelating: metal). Ethylene glycol ($C_2H_6O_2$, Aldrich $>99.9\%$) was then added in a chelating/alcohol mass ratio of 60:40 in order to form the polymeric gel. Finally, ethylenediamine ($C_2H_8N_2$, Aldrich $>99.9\%$) was added for a pH adjustement of 3 for Co_2MnO_4 and, because of the Bi presence, a pH of 5 for $Bi_xCo_{2-x}MnO_4$. Pyrolisis was performed at 400 °C for 4 h, followed by successive annealings at 850 °C–24 h, 1000 °C–12 h and 1100 °C–12 h, with intermediate grinding.

Powder X-Ray diffraction (XRD) data were obtained at room temperature on a Bruker D8 Discover diffractometer with Cu-$K_{\alpha 1}$ radiation, $\lambda=1.5406$ Å, selected by a Ge(111) monochromator. The data were collected in the 5°–80° 2θ range with a 0.02° step, in continuous mode. Rietveld refinement was performed using the GSAS program to adjust the structural parameters, the preferred orientation and get quantitative phase analysis [22]. A Thompson–Cox–Hasting pseudo-Voigt profile was used in order to resolve the instrumental, strain and size contributions to the peak broadening. The microstructure and particles size were observed by scanning electron microscopy (SEM) on a JEOL JSM 6301F equipment, whereas the X-Ray energy dispersion spectra (EDS) were collected on a JEOL JSM 6400—OXFORD detector. Magnetic measurements of Co_2MnO_4 and $Bi_xCo_{2-x}MnO_4$ samples were performed on a Quantum Design MPMS-XL5 SQUID (Superconducting Quantum Interference Device) magnetometer. All samples were studied under identical conditions. Magnetization as a function of temperature was carried out on samples in the zero-field-cooled (*ZFC*) and field-cooled (*FC*) modes under an applied field of 100 Oe. Initially, the specimen is cooled down to 5 K in the absence of field, then a magnetic field (100 Oe) is applied and the magnetization M is measured while the temperature increases up to 400 K (*ZFC* mode). At last, the magnetization is measured when the specimen is cooled back to 5 K (*FC* mode). The magnetic susceptibility, $\chi=M/H$, is evaluated at the paramagnetic state, well above the magnetic transition temperature, under an applied field of 10 kOe. Magnetization $M(H)$ loops were recorded at 10 K between -50 kOe and 50 kOe.

3. Results and discussion

X-Ray diffraction patterns obtained at room temperature for $Bi_xCo_{2-x}MnO_4$ samples, with $x=0.0$, 0.1, 0.2 and 0.3, in polycrystalline powder form, are shown in Fig. 1. Co_2MnO_4 presented a cubic spinel structure with no secondary phases and in excellent agreement with the *JCPDS-ICDD* card no. 84-0482, The *Fd*3*m* (227) space group, and unit cell parameter $a=8.271$ Å. X-Ray patterns of all $Bi_xCo_{2-x}MnO_4$ materials, presented the same peaks as the non-doped sample, confirming their cubic spinel structure. All samples showed excellent crystallinity, well-defined peaks and higher intensity from the (311) plane. Fig. 2 shows the XRD reflections for the Co_2MnO_4 compound, corresponding to the (111), (220), (311), (222), (400), (4 2 2), (333), (440), (531), (620), (533) and (622) crystallographic planes. All peaks were fitted using the Thomson–Cox–Hasting pseudo-Voigt profile function. The peak profile was fitted by the double-Voigt function with a Gauss and Lorentz broadenings [23]. The unit cell parameter, the zero point of detector, the scale factor and the background terms were optimized, the last one being fitted by a *Chebyschev* polynomial. Based on least-squares minimization

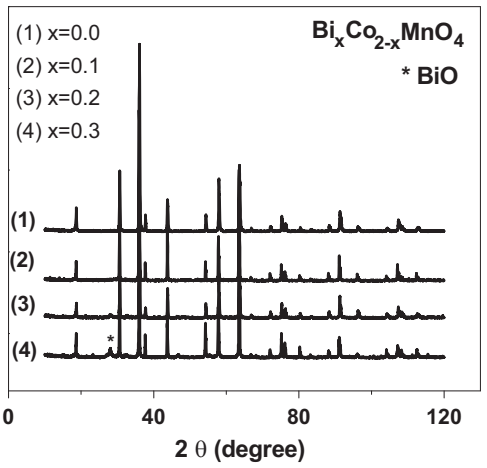

Fig. 1. X-ray diffraction patterns for $Bi_xCo_{2-x}MnO_4$ ($x=0.0$, 0.1, 0.2 and 0.3) samples heat-treated at 1100 °C for 12 h. Indexed in a cubic spinel *Fd3m* (227) space group. Asterisk indicates spurious phase.

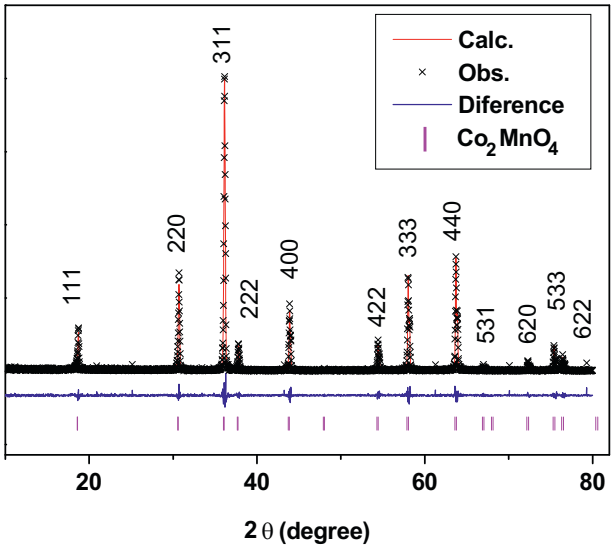

Fig. 2. Rietveld refinement for the Co_2MnO_4 sample. Refinement factors: $R_{wp}=0.1699$, $R_{exp}=0.1121$and $\chi^2=1.5160$ obtained by the GSAS program.

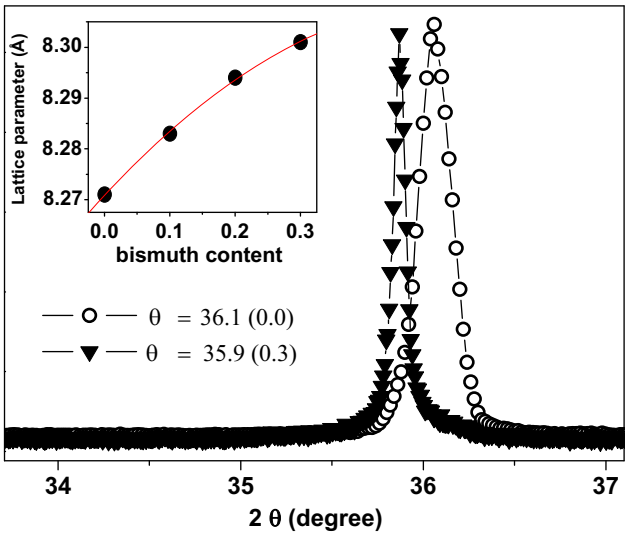

Fig. 3. Detailed X-ray diffraction patterns for Co_2MnO_4 and $Bi_{0.3}Co_{1.7}MnO_4$ showing the shift of the peak corresponding to the (311) reflection towards lower 2θ. Inset shows the variation of the lattice parameter '*a*' with the Bi content '*x*'.

criteria, the XRD data of the Co_2MnO_4 material was successfully fitted, obtaining reasonable values for the weighted profile *R*-factor ($R_{wp}=0.1699$), the expected *R*-factor ($R_{exp}=0.1121$) and the goodness of fit ($\chi^2=1.5160$). Knowing that Bi and Co have quite different ionic radii, it is remarkable that there is no change in symmetry when Co is substituted by Bi, except a shift toward lower 2θ angles of the peaks associated to the crystallographic planes. Fig. 3 compares the peak corresponding to the (3 1 1) plane of the $x=0.0$ and $x=0.3$ materials, centered at 36.1 and 35.9 2θ values, respectively. The observed shifts can be explained by the larger ionic radius of Bi compared to Co, and thus they are directly related to the Bi content. The inset, Fig. 3 shows a non-linear variation of the lattice parameter, increasing monotonously with the bismuth content, from 8.271 Å, for Co_2MnO_4, to 8.283 Å, 8.294 Å, 8.301 Å, for $Bi_{0.1}Co_{1.9}MnO_4$, $Bi_{0.2}Co_{1.8}MnO_4$, and $Bi_{0.3}Co_{1.7}MnO_4$, respectively. Taking into account the large difference of ionic radii between Bi^{3+}, Co^{3+} and Mn^{3+} (1.17 Å, 0.65 Å and 0.78 Å, respectively), it is observed that from $x=0.2$ and above, the system approaches a solubility limit and does not follow Vegard's law [24]. Such a large difference between the ionic radii is probably the reason of the presence of a minor BiO spurious phase (*JCPDS-ICDD* card no. 75-0995), easily formed and evidenced in the XRD pattern of the $Bi_{0.2}Co_{1.8}MnO_4$ and the $Bi_{0.3}Co_{1.7}MnO_4$ materials (Fig. 1). Peaks corresponding to this spurious phase are more pronounced in samples in which bismuth is present in larger percentuals, as in the case of the $Bi_{0.3}Co_{1.7}MnO_4$ sample. Based on the XRD data and SEM observations, we could estimate their presence to a 0.5–2 wt%, for x(Bi) contents varying from $x=0.1$ to $x=0.3$, respectively. Scanning electron microscopy (SEM) images of $Bi_xCo_{2-x}MnO_4$ powders calcined at 1100 °C, are shown in Fig. 4 for $x=0.0$ and $x=0.3$. The micrograph of $Bi_{0.3}Co_{1.7}MnO_4$, taken at 10,000X resolution, shows the presence of the undesirable BiO phase at the grains borders although in negligible amounts. From the morphological point of view, the $Bi_xCo_{2-x}MnO_4$ samples displayed different patterns: in the examples shown in Fig. 4, the Co_2MnO_4 presented uniform grain morphology, with grains of relative regular shape homogeneously distributed over the surface, even though larger grains appear occasionally, whereas the $Bi_{0.3}Co_{1.7}MnO_4$ material exhibited a dense structure, with larger grain size resulting in a much narrower XRD peak, as evidenced in Fig. 3.

The magnetic properties of the spinel oxides were investigated in order to compare the magnetic behavior of the parent compound Co_2MnO_4 with those of the Bi-doped specimens. Fig. 5 shows the temperature dependence of the zero-field-cooled/field-cooled (*ZFC/FC*) magnetization cycles of all four samples $Bi_xCo_{2-x}MnO_4$ ($x=0.0$, 0.1, 0.2 and 0.3) in the presence of an applied magnetic field of 100 Oe. Their overall behavior is typical of ferrimagnetic materials with large negative Curie–Weiss temperatures and well-defined maxima during the *ZFC* warming followed by an *FC* magnetization which increases continuously with decreasing temperature. These facts indicate different types of magnetic interactions between ions occupying the A and B sublattices, in particular: intrasite J_{AA} and J_{BB} and intersite J_{AB} exchange interactions [15]. From these, the J_{AA} interactions at the tetrahedral sites between Co^{2+}–Co^{2+} moments tend to cancel out since the cobalt spins point into opposite directions in an antiferromagnetic ordered state, as it is the case in the Co_3O_4 compound [25]. By replacing Co by Mn at the octahedral site of the cobalt oxide Co_3O_4 spinel to form the mixed cobalt-manganese spinel Co_2MnO_4, a partial oxidation of Mn^{3+} into Mn^{4+} occurs [26], which is accompanied by ferromagnetic Mn^{3+}–Mn^{4+} interactions. These interactions are responsible of the large increase of the FC magnetization in Co_2MnO_4, as shown in Fig. 5. Further substitution of Co by Bi to form the $Bi_xCo_{2-x}MnO_4$ system makes important changes in the distribution of charges and, subsequently, on the exchange interactions between octahedral and tetrahedral sites. When the Co ions are replaced by the Bi ions at the octahedral site, the oxygen octahedra distorts because of the much larger ionic radius of Bi compared to the radius of Co [6]. Another factor to be considered is the Jahn–Teller effect of the Mn^{3+} ion, also at the origin of structural distortions and subsequent modifications of the super-exchange magnetic interactions through the control of orbital overlaps. Such distortion provokes a deviation of the antiparallel Co^{2+} spins situated at the tetrahedral position, in a canted-like AFM alignment and enhancing the ferromagnetic component. As shown in Fig. 5, the absolute value of the *FC* magnetization at $T=0$ (extrapolation of the *FC* curve) increases by a factor of 2, from 20.9 emu/mol up to 37.0 emu/mol when *x* goes from 0 to 0.3 (Table 1). Some authors forwarded the idea of a magnetic frustration at the tetrahedral site due to the structural distortions of the oxygen octahedra [6]. This is a plausible idea regarding the very large Curie–Weiss temperatures (Table 1). However, the frustration parameter $f=|\theta_{CW}|/T_C$, which is a criterion for

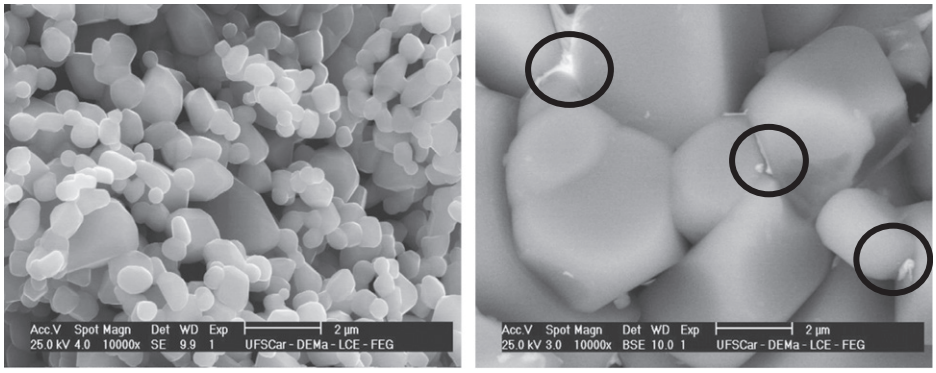

Fig. 4. Scanning electron microscopy (SEM) image for the Co_2MnO_4 and $Bi_{0.3}Co_{1.7}MnO_4$ samples both heat-treated at 1100 °C for 12 h. Circles show the presence of bismuth oxide.

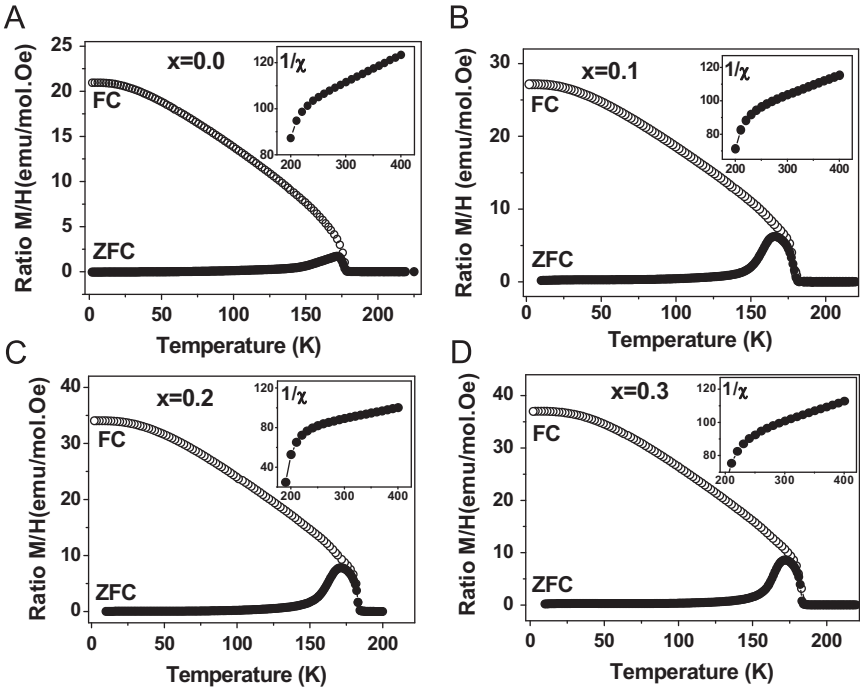

Fig. 5. Temperature dependence of the DC magnetization for $Bi_xCo_{2-x}MnO_4$ (A) $x=0.0$, (B) $x=0.1$, (C) $x=0.2$ and (D) $x=0.3$, under $H=100$ Oe. Insets show the inverse magnetic susceptibility under $H=10$ kOe.

Table 1
Magnetic parameters for $Bi_xCo_{2-x}MnO_4$ ($x=0.0$, 0.1, 0.2 and 0.3). T_C: transition temperatures, T_{max}: temperature values at the *ZFC* magnetization peaks, Θ_{CW}: Curie-Weiss temperatures, μ_{eff}: effective moments, H_C: coercive fields values, M_{FC}: extrapolation of FC curves at $T=0$, and $M_{50\ kOe}$: magnetization measured at $H=50$ kOe.

$Bi_xCo_{2-x}MnO_4$	T_C (K)	T_{max} (K)	Θ_{CW} (K)	μ_{eff} (μ_B)	H_C (Oe)	M_{FC} ($T=0$) (emu/mol)	$M_{50\ kOe}$ (μ_B)
0.0	180	172	−630	8.2	3360	20.9	0.63
0.1	182	166	−552	8.1	1880	27.2	0.83
0.2	185	171	−520	8.2	1570	34.0	1.05
0.3	184	172	−540	8.2	1440	37.0	1.07

magnetic frustration if $f > 10$ [27], is of the order of 3–3.5 in our present case and we may conclude then that the main mechanisms to describe the magnetism of these Bi-doped spinels are related to the J_{AB} intersite interactions between Co^{2+}–Mn^{3+}, Co^{2+}–Mn^{4+}, and intrasite ferromagnetic exchange Mn^{3+}–Mn^{4+}.

Other features can be highlighted from Fig. 5, in particular the magnetic ordering temperature T_C, evaluated from the linear extrapolation of the *FC* curve to the *x*-axis, which shows a slight increase with the bismuth content, going from 180 K up to 185 K, for *x* increasing from 0 up to 0.3 Bi. Additionally, the *ZFC* maxima, associated to the antiferromagnetic interactions, show qualitative changes when Bi is incorporated into the lattice. In the parent compound Co_2MnO_4, the peak is narrow and asymmetric, presenting a maximum value at $T=T_N=172$ K. In contrast, the *ZFC* curves for the $x=0.1$, 0.2 and 0.3 Bi samples exhibit wide maxima with quite symmetric variations, at $T=T_{max}$ around 166 K, 171 K and 172 K, respectively (Table 1). This fact can be related directly to the bismuth cation which, because of its large ionic radius, distorts the spinel structure, modifying the magnetic interactions between the A and B sub-lattices.

The magnetic susceptibility was studied in the paramagnetic state from 200 K up to 400 K, under an applied field of 10 kOe. Insets in Fig. 5 show the inverse susceptibility as a function of temperature for all four samples. Data were fitted by a Curie–Weiss law $\chi=C/T-\theta_{CW}$ in the range (300–400 K), where data was quite linear (correlation factors close to unity). Values of the Curie-Weiss temperatures (Θ_{cw}) were obtained from the extrapolation of the high temperature region of the inverse

susceptibility and are given in Table 1. These values were found to be largely negative, with all graphs showing a strong curvature at the approach of the magnetic transition, typical of the ferrimagnetic behavior of a material composed of two magnetic sublattices A and B [28]. This observation confirms the coexistence of antiferromagnetic (AFM) and ferromagnetic (FM) contributions as observed in the *ZFC*/*FC* cycles. Presence of Bi^{3+} at the octahedral site modifies the AFM and FM interactions. The AFM component is largely reduced, as seen by the increase of the negative Curie–Weiss temperature Θ_{cw}, from −630 K (for $x=0$) up to about −540 K, in the Bi-doped samples. On the other hand, the effective moment μ_{eff} does not undergo considerably changes, showing almost no dependence with the Bi-content (Table 1). This is a remarkable result if one considers that part of the cobalt ions is substituted in the $Bi_xCo_{2-x}MnO_4$ samples. However, based on the valence fluctuations which may undergo both Mn and Co ions, it is quite possible that the contributions from each magnetic species compensate each other [$(\mu_{Co}^{2+})=(\mu_{Mn}^{4+})=3.87\ \mu_B$; $(\mu_{Co}^{3+})=(\mu_{Mn}^{3+})=4.90\ \mu_B$], resulting into an almost constant value ($\mu_{eff}\sim 8.2\ \mu_B$) for all materials. On the other hand, under the assumption that Bi^{3+} substitutes the low-spin Co^{III} ion located at the octahedral site, both being nonmagnetic, then no changes are expected on the overall paramagnetic moment. Based on the neutron diffraction data of Bordeneuve et al. [26], we may propose a charge balance of the type $Co^{2+}[Co_x^{2+}Co_{1-x}^{III}Mn_{1-x}^{3+}Mn_x^{4+}]O_4$ for Co_2MnO_4, and $Co^{2+}[Co_x^{2+}\left(Bi^{3+},Co^{III}\right)_{1-x}Mn_{1-x}^{3+}Mn_x^{4+}]O_4$ for the slightly doped spinels.

Hysteresis loops were performed at 10 K with the magnetic field varying from −50 kOe up to +50 kOe. The positive part of these loops is illustrated in Fig. 6 for all samples. The coercive field H_C undergoes a noticeably change when doping the Co_2MnO_4 material with bismuth (Table 1), showing a tendency toward a constant limit when increasing the bismuth content (inset, Fig. 6). Two possible reasons can be forwarded. Firstly, the ferromagnetic interactions have been optimized and no further variation will result in the ordered state. Secondly, a saturation limit is reached at x(Bi) ~0.2–0.3, as suggested by the evolution of the lattice parameter of the cubic spinel structure (inset, Fig. 3). Indeed, because of the large size of the Bi ion, a limit seems to be attained, as seen for $Bi_xCo_{2-x}MnO_4$ samples synthesized by solid state reaction [16], and further modifications become negligible in comparison to the large increase observed at x(Bi)=0.1 and 0.2, with respect to the parent compound Co_2MnO_4 ($x=0.0$). Further comparison is made in Fig. 7, which zooms the M(H) loops for all

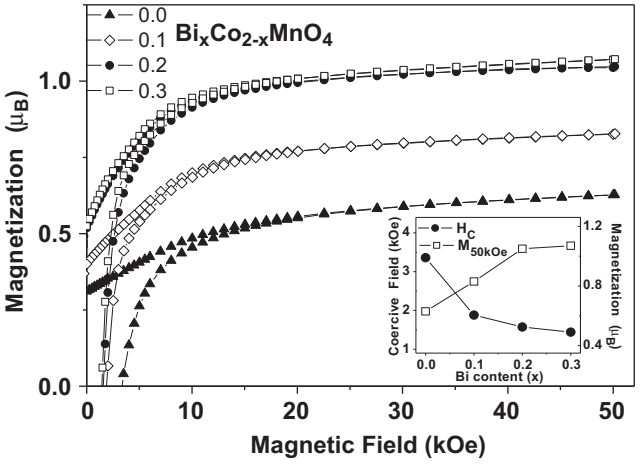

Fig. 6. Magnetization as a function of the applied field for the $Bi_xCo_{2-x}MnO_4$ ($x=0.0$, 0.1, 0.2 and 0.3) materials, measured at $T=10$ K with magnetic fields varying between −50 kOe and +50 kOe. Inset: coercive field (left) and magnetization $M_{50\ kOe}$ measured at $H=50$ kOe (right), versus Bi content.

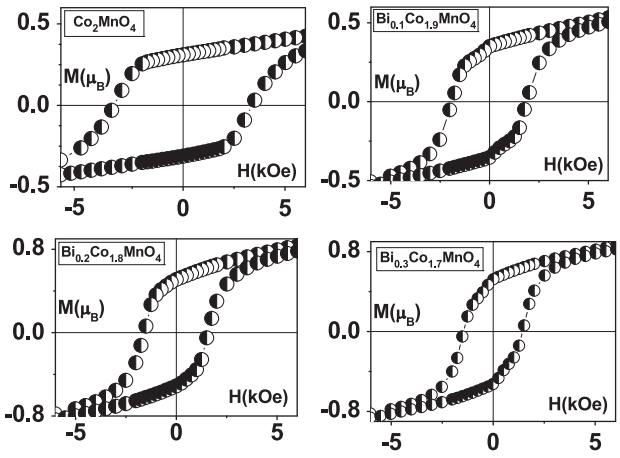

Fig. 7. Details of the magnetization loops of the $Bi_xCo_{2-x}MnO_4$ ($x=0.0$, 0.1, 0.2 and 0.3) materials measured at $T=10$ K, with magnetic field varying between −50 kOe and +50 kOe.

samples. It is quite evident that the strongest modification occurs when doping the parent compound with x(Bi)=0.1 content, the coercive field H_C being reduced by a factor of 2 between $x=0.0$ and $x=0.1$.

An important point should be remarked in both Figs. 6 and 7 concerning the absolute value of the magnetization, $M_{50\ kOe}$, measured at the highest field. The spins of the Mn and Co ions align under the influence of an increasing magnetic field, almost saturating at 50 kOe (Table 1). With Bi (a non-magnetic ion) entering in specific positions in the crystallographic structure, the cobalt sublattice is disturbed and so, the antiferromagnetic interactions associated to it become weaker. As a result, a parallel alignment in the same direction of the applied fields is favored, and the magnetization $M_{50\ kOe}$ increases (inset, Fig. 6, right-hand axis). The low values of the magnetization $M_{50\ kOe}$, reaching at the most 1.0 μ_B, are in fact due to negative interactions between Co^{2+} spins ($gS=3\ \mu_B$) and Mn^{3+} spins ($gS=4\ \mu_B$), suggesting that two ferromagnetic sublattices coexist, with antiferromagnetic interactions between them. In addition, the canting phenomenon which probably takes place in the tetrahedral sublattices [13], will contribute with an additional ferromagnetic component. Thus, when partially substituting Co^{III} by nonmagnetic bismuth, the antiferromagnetic interactions are minimized, and the ferromagnetic interactions become predominant. Neutron diffraction experiments are in progress and should shade further light to this assertion.

4. Conclusions

The structural and magnetic properties of cobalt–manganese Co_2MnO_4 doped with Bi ($Bi_xCo_{2-x}MnO_4$, x varying from 0.0 to 0.3) have been investigated. Materials were synthesized using a modified polymeric precursors approach and structurally characterized by XRD and Rietveld refinement. A cubic spinel structure was obtained, with bismuth occupying the cobalt positions and Co^{2+}/Co^{III} and Mn^{3+}/Mn^{4+} ions being distributed over both tetrahedral and octahedral sites. XRD data showed polycrystalline materials with excellent cristallinity and well defined peaks although minute amounts of nonmagnetic oxides were present in $Bi_{0.2}Co_{1.8}MnO_4$ and $Bi_{0.3}Co_{1.7}MnO_4$. SEM images showed important changes in the grains morphology, increasing the particles size by one order of magnitude depending on the Bi-content.

Antiferromagnetic and ferromagnetic interactions coexist in these materials, as shown by the *ZFC*/*FC* cycles and the high temperature magnetic susceptibility, both being described by

ferrimagnetic behavior. Presence of Bi did not alter ferrimagnetism but, the magnetic ordering temperature T_C, the magnetization value $M_{50\ kOe}$ measured at high fields and the field-cooled M_{FC} magnetization were enhanced with Bi doping. The $M(H)$ loops measured at 10 K showed large loop areas for Co_2MnO_4, steadily decreasing with Bi doping. Substitution of Co^{III} by Bi^{3+} makes important changes in the distribution of charges, being responsible of the valence fluctuation Mn^{3+}–Mn^{4+} and its associated ferromagnetic exchange interactions, together with exchange interactions between tetrahedral and octahedral sites. As a result, the Co^{2+}–Co^{2+} AFM interactions become weaker with higher Curie–Weiss temperatures, while ferromagnetism, due to Mn^{3+}–Mn^{4+} exchange interactions, is enhanced.

Acknowledgments

Authors are thankful to FAPESP GRANT 2007/08072-0. The authors also acknowledge the bilateral exchange programs France-Brazil CAPES-COFECUB, project no. 706/11. M.E. Santos and R.A. Ferreira in a Joint Ph.D. International Program, UNESP-Université de Rennes 1.

References

[1] D. Khomskii, Physics 20 (2009) 2.
[2] A.H. Nicola, Journal of Physical Chemistry B 104 (2000) 6694.
[3] D.-C. Jia, J.-H. Xu, H. Ke, W. Wang, Y. Zhou, Journal of the European Ceramic Society 29 (2009) 3099.
[4] J. Rodriguez-Carvajal, G. Rousse, C. Masquelier, M. Hervieu, Physical Review Letters 81 (1998) 4660.
[5] N.A. Spaldin, S. Cheong, R. Ramesh, Physics Today 63 (2010) 38.
[6] B.L. Ahuja, A. Dashora, N.L. Heda, S. Tiwari, N.E. Rajeevan, M. Itou, Y. Sakurai, R. Kumar, Applied Physics Letters 97 (2010) 212502.
[7] A.L.G. Prette, M. Cologna, V. Sglavo, R. Raj, Journal of Power Sources 196 (2011) 2061.
[8] A. Petric, H. Ling, Journal of the American Ceramic Society 90 (2007) 1515.
[9] S. Guillemet-Fritsch, C. Tenailleau, H. Bordeneuve, A. Rousset, Advances in Science and Technology 67 (2010) 143.
[10] E. Ríos, P. Lara, D. Serafini, A. Restovic, J.L. Gautier, Journal of the Chilean Chemical Society 55 (2010) 2.
[11] N.E. Rajeevan, R. Kumar, D.K. Sukla, P.P. Pradyumnan, S.K. Arora, I.V. Shvets, Materials Science and Engineering B 163 (2009) 48.
[12] R. Kumar, S.K. Arora, I.V. Shvets, N.E. Rajeevan, P.P. Pradyumnan, D.K. Shukla, Journal of Applied Physics 105 (2009) 07D910.
[13] N.E. Rajeevan, P.P. Pradyumnan, R. Kumar, D.K. Shukla, S. Kumar, A.K. Singh, S. Patnaik, S.K. Arora, I.V. Shvets., Applied Physics Letters 92 (2008) 102910–102911.
[14] K. Oka, M. Azuma, W. Chen, H. Yusa, A.A. Belik, E.T. Muromachi, M. Mizumaki, N. Ishimatsu, N. Hiraoka, M. Tsujimoto, M.G. Tucker, J.P. Attfield, Y. Shimakawa, Journal of the American Chemical Society 132 (2010) 9438.
[15] N.E. Rajeevan, R. Kumar, D.K. Shukla, R.J. Choudhary, P. Thakur, A.K. Singh, S. Patnaik, S.K. Arora, I.V. Shvets, P.P. Pradyumnan, Journal of Magnetism and Magnetic Material 323 (2011) 1760.
[16] N.E. Rajeevan, R. Kumar, D.K. Shukla, P. Thakur, N.B. Brookes, K.H. Chae, W.K. Choi, S. Gautam, S.K. Arora, I.V. Shvets, P.P. Pradyumnan., Journal of Physics: Condensed Matter 21 (2009) 406006.
[17] M.B. Salamon, Reviews of Modern Physics 73 (2001) 583.
[18] P.N. Lisboa-Filho, M. Bahout, P. Barahona, C. Moure, O. Peña, Journal of Physics and Chemistry of Solids 66 (2005) 1206.
[19] A. Moure, T. Hungría, A. Castro, J. Galy, O. Peña, I. Martínez, J. Tartaj, C. Moure, Ceramics International 38 (2012) 1507.
[20] M. Motta, C.V. Deimling, M.J. Saeki, P.N. Lisboa-Filho, Journal of Sol-Gel Science and Technology 46 (2008) 201.
[21] P.N. Lisboa, A.W. Mombrú, H. Pardo, W.A. Ortiz, E.R. Leite., Journal of Physics and Chemistry of Solids 64 (2003) 583.
[22] H.M. Rietveld, Journal of Applied Crystallography 2 (1969) 65.
[23] R.A. Young., The Rietveld Method. IUCr Monographs on Crystallography—5th International Union of crystallography, Oxford University Press, 1993.
[24] J.F.Q. Rey, E.N.S. Muccillo, Cerâmica 48 (2002) 307.
[25] W.L. Roth, Journal of Physics and Chemistry of Solids 25 (1964) 1.
[26] H. Bordeneuve, C. Tenailleau, S. Guillemet-Fritsch, R. Smith, E. Suard, A. Rousset, Solid State Sciences 12 (2010) 379.
[27] P. Schiffer, A.P. Ramirez., Condensed Matter Physics (Rapid Communication) 10 (1996) 21.
[28] A. Herpin, Théorie du magnétisme, Presses universitaires de France, Paris—VI, 1968.